Progress In Electromagnetics Research, Vol. 143, 243–261, 2013

DUAL-BAND CIRCULAR POLARIZER AND ASYMMETRIC SPECTRUM FILTER USING ULTRATHIN COMPACT CHIRAL METAMATERIAL

He-Xiu Xu[1, 2, *], Guang-Ming Wang[1], Mei Qing Qi[2], and Tong Cai[1]

[1]Missile Institute, Air Force Engineering University, Xi'an 710051, Shaanxi, People's Republic of China

[2]State Key Laboratory of Millimeter Waves, Southeast University, Nanjing 210096, People's Republic of China

Abstract—A compact chiral metamaterial is proposed and comprehensively investigated that can achieve circularly polarized wave emission from linearly polarized incident wave (giant circular dichroism) over dual bands and near Diodelike asymmetric transmission of linearly polarized waves. The chiral metamaterial also features exceptionally strong optical activity. For verification, two proof-of-concept slab samples are designed, fabricated and measured at microwave frequencies. Numerical and experimental results agree well, indicating that the former dual-band circular polarizer features high conversion efficiency around 8.1 and 9.9 GHz in addition to large polarization extinction ratio of more than 16 dB, while the latter chiral sample enables the near 90% cross-polarization transmission in one direction and almost 10% transmission in the opposite direction. The block "meta-atom" that utilized to build the ultrathin CMM slab is less than $\lambda_0/6.73$ evaluated at operating frequency. Good performances of the two chiral slabs with simple and compact package suggest promising applications in the circular polarizers (circulators) and transparent linear polarization transformers or spectrum filters (isolators) that need to be interpreted with other compact devices.

1. INTRODUCTION

Recently, chiral metamaterials (CMMs) have attracted increasing attention from the microwave frequency band to optical spectrum

Received 30 September 2013, Accepted 28 October 2013, Scheduled 1 November 2013

* Corresponding author: He-Xiu Xu (hxxuellen@gmail.com).

due to their unique electromagnetic (EM) properties and a wider set of functionalities such as giant optical activity [1], elliptical or circular dichroism [2], giant gyrotropy [3], negative refraction without simultaneous negative permittivity and permeability [4–9], and asymmetric transmission [10–15], etc. The unusual polarization functionalities and chirality not found in natural medium arise from the magneto-electric cross coupling of chiral structures due to their bianisotropy and lack of any mirror symmetry. After the extensive theoretical or numerical studies, and experimental realizations, there have been many efforts tending toward the practical applications of the CMMs in manipulating the polarization states of EM wave [16–29], polarization spectral filtering [30], improving the gain and axial ratio of circularly polarized antennas [31], subwavelength focusing and imaging [32], as well as microwave absorbers [33]. A set of circular polarizers [16–24] and pure linear polarization rotators [25–29] have been intensively reported.

Among them, several chiral structures have been available to tailor the cross coupling between electric and magnetic fields such as the commonly utilized U-shaped structures [1, 15, 21, 29], conjugated metallic pairs and conjugated gammadion resonators combining cut-wire pairs [27, 28], twisted rosettes [2, 3, 5], cross-wire structure (gammadion) and its complementary variations [9, 11, 20, 31], twisted foil structure [7, 26], L-shaped chiral structure [8], fish-scale pattern [10, 11], twisted split ring resonators (SRRs), twist Hilbert patterns, and twisted complementary SRRs with symmetric or asymmetric geometry [12–14, 23, 24, 30, 33], Metallic helix array[16, 18], stacked nanorod arrays [19], twist arc structure [22], and I-shaped structure [25]. However, most "meta-atoms" or "meta-molecule" of CMMs are extremely large, this is especially true when arrange the four U-shaped rings in four-fold rotational symmetry (C4) to obtain the optical activity insensitive to the linear polarization of the incident wave. In this case, Bragg scattering and Wood anomalies enhance considerably. In fact, many chiral structures lie in between photonic crystals and effective media, refraining designers from retrieving effective material parameters for exactly tailoring the EM parameters [16]. Compact CMMs with small building blocks or lower operation frequencies are extremely useful to address these issues and reduce the fabrication costs. To the authors' best knowledge, in addition to [23], another two research groups have attempted to achieve this goal most recently [9, 24]. However, the meandered strategy in the cross-wire chiral structures [9] still provides insufficient miniaturization.

In this paper, we provide an alternative and efficient strategy

to reduce the size of meta-atoms of CMMs inspired from the recent work toward this goal by some of the authors [34–36] and investigate two fundamental aspects of the resulting chiral medium, advancing a step from the effective medium concept. The two-turn spiral structure is utilized and the concept can be extended to three turns or multiple turns for an ultra-compact package. Although the concept of spiral "meta-atom" was proposed in magnetic materials [37], it to the best of our knowledge has never been explored in the CMM, to say nothing of the appealing behaviors of high-efficiency circular polarization conversion over dual bands and near diodelike resonant asymmetric transmission at normal incidence in this work. Moreover, the resonant frequencies of the planar structure can be manipulated at arbitrary frequencies due to the geometry scalability.

2. FUNDAMENTALS, THEORY AND DESIGN

To begin with, we first present briefly some fundamentals and theory of the CMMs in the design of circular polarizer and linear polarization rotator (with asymmetric transmission for linear polarization as a special case) and then establish the design criterion for the proposed CMM to achieve those goals. Under the Cartesian coordinate system, the decomposed components of the transmitted EM waves E_x^t and E_y^t through certain slab of a chiral medium associate with the linearly incident waves E_x^i and E_y^i through four linear transmission components (the complex Jones matrix).

$$\begin{pmatrix} E_x^{tf} \\ E_y^{tf} \end{pmatrix} = \begin{bmatrix} t_{xx}^f & t_{xy}^f \\ t_{yx}^f & t_{yy}^f \end{bmatrix} \begin{pmatrix} E_x^{if} \\ E_y^{if} \end{pmatrix} \tag{1}$$

$$\begin{pmatrix} E_x^{tb} \\ E_y^{tb} \end{pmatrix} = \begin{bmatrix} t_{xx}^b & t_{xy}^b \\ t_{yx}^b & t_{yy}^b \end{bmatrix} \begin{pmatrix} E_x^{ib} \\ E_y^{ib} \end{pmatrix} \tag{2}$$

where the subscripts x and y denote the polarization states of the transmitted/reflected wave and incident wave components and the subscripts f and b represent forward and backward propagation of the EM wave. For the reciprocal chiral system, we have $t_{xx}^f = t_{xx}^b = t_{yy}^f = t_{yy}^b$, $t_{xy}^f = -t_{yx}^b$, and $t_{yx}^f = -t_{xy}^b$ [11]. The two orthogonal polarization eigenstates right handed circularly polarized (RCP) (E_+^t) and left handed circularly polarized (LCP) (E_-^t) EM waves associate with the two incident orthogonal linearly polarized components as [24]

$$\begin{pmatrix} E_+^t \\ E_-^t \end{pmatrix} = \frac{1}{\sqrt{2}} \begin{pmatrix} T_{+x} & T_{+y} \\ T_{-x} & T_{-y} \end{pmatrix} \begin{pmatrix} E_x^i \\ E_y^i \end{pmatrix} = \frac{1}{\sqrt{2}} \begin{bmatrix} t_{xx}+it_{yx} & t_{xy}+it_{yy} \\ t_{xx}-it_{yx} & t_{xy}-it_{yy} \end{bmatrix} \begin{pmatrix} E_x^i \\ E_y^i \end{pmatrix} \tag{3}$$

where T_{+x}, T_{-x}, T_{+y}, and T_{-y} are four transformation coefficients in the circular polarization base. Note that the above equation

is suitable for both cases of forward and backward propagation. Observation of Eq. (3) indicates the capability of the CMM to transform an EM wave with linear polarization to that with circular polarization. As a circular polarizer for x or y-polarized incidence, the ratio $|t_{yx(xy)}|/|t_{xx(yy)}|$ should be near unity while the phase difference $\varphi(t_{yx(xy)}) - \varphi(t_{xx(yy)})$ should be in the vicinity of $\pm 90^\circ$ at the operation frequency. This enables the substantially large or small difference (polarization extinction ratio) between the RCP and LCP wave calculated by $20\log_{10}(|T_{+x(y)}|/|T_{-x(y)}|)$ and thus strong circular dichroism. Moreover, the transmission coefficients and conversion efficiency should be as high as possible. As a linear polarization rotator, the chiral slab should convert one linear polarization completely or near completely to its cross polarization and thus giant optical activity can be envisioned. The polarization azimuth rotation angle θ and ellipticity η of emitted wave can be calculated by the following equations.

$$\theta = [\arg(E_+) - \arg(E_-)]/2 \tag{4}$$

$$\eta = \arctan\frac{|E_+| - |E_-|}{|E_+| + |E_-|} \tag{5}$$

where θ is defined as the major axis of the ellipse and the x-axis, and η describes the polarization of the wave. Under the circular polarization base, the T matrix that connecting the incident and transmitted circularly polarized wave in forward propagation can be transformed from the linear transmission coefficients

$$\begin{aligned} T^f_{circ} &= \begin{pmatrix} T_{++} & T_{+-} \\ T_{-+} & T_{--} \end{pmatrix} \\ &= \frac{1}{2}\begin{pmatrix} t_{xx} + t_{yy} + j(t_{xy} - t_{yx}) & t_{xx} - t_{yy} - j(t_{xy} + t_{yx}) \\ t_{xx} - t_{yy} + j(t_{xy} + t_{yx}) & t_{xx} + t_{yy} - j(t_{xy} - t_{yx}) \end{pmatrix} \end{aligned} \tag{6}$$

For the backward propagation, the T matrix in a reciprocal system becomes [11]

$$T^b_{circ} = \begin{pmatrix} T_{++} & T_{-+} \\ T_{+-} & T_{--} \end{pmatrix} \tag{7}$$

The asymmetric effects of EM waves are caused by the partial conversion of the incident EM wave into opposite polarization and are characterized by the Δ parameter defined as the difference between the transmittances in the two opposite propagation directions ($+z$ and $-z$). For circularly polarized waves, the total transmission through the chiral slab defined by $T_+ = T_{++} + T_{+-}$ and $T_- = T_{--} + T_{-+}$ is different for either opposite handedness or opposite direction of incidence, yielding the nonzero value of the following equations

$$\Delta T = T_{++} - T_{--} \neq 0, \quad \Delta^+_{circ} = |T_{+-}|^2 - |T_{-+}|^2 = -\Delta^-_{circ} \neq 0 \tag{8}$$

where ΔT is the absolute difference in the co-polarization transmission of the RCP and LCP waves, and Δ^{+}_{circ} represents the absolute difference in the cross-polarization transmission of forward or backward propagation. For linearly polarized wave, the Δ parameter is calculated through

$$\Delta^{x}_{lin} = |t_{yx}|^2 - |t_{xy}|^2 = -\Delta^{y}_{lin} \tag{9}$$

Therefore, Eqs. (6)–(9) indicate that the asymmetric transmission for linear and circular polarization in a reciprocal semiplanar chiral slab simultaneously requires $|t_{xy}| \neq |t_{yx}|$. For a criterion set for asymmetric transmission of linearly polarized waves only, additional requirement of $t_{xx} = t_{yy}$ should be compulsorily satisfied. To go step further for a perfect or near diodelike asymmetric transmission of linearly polarized waves, we require that $t_{xy} \approx 1$ and $t_{yx} \approx 0$ or $t_{xy} \approx 0$ and $t_{yx} \approx 1$ [15] in this work. The large asymmetric transmission for the linear polarization also incurs the quite distinguished total transmission of x or y-polarized EM wave defined by $T_x = t_{xx} + t_{yx}$ and $T_y = t_{yy} + t_{xy}$, respectively along two opposite directions of propagation. Note that similar polarization and directional asymmetry can be seen in reflection and in this work we mainly concentrate on the transmission case.

With the purpose of asymmetric transmission and giant chirality, the mirror symmetry breaking along the propagation direction is the unique route, which enables the lack of structural mirror symmetry. Previous SRR or complementary SRR structure still possesses certain line of mirror symmetry in the plane normal to the propagation and the potential for further miniaturization is still available. These drawbacks make them not good candidates in this area. An asymmetry was recently introduced in both arc and gaps so that the resulting metamaterial has no line of mirror symmetry [10, 14, 30], enabling the asymmetric transmission of circularly polarized wave, however, this leads to exceptionally large meta-atoms.

Figures 1(a) and (b) show the schematic and geometrical parameters of the proposed meta-atom that is utilized as the basic building block of the CMM circular polarizer and the chiral slab for near Diodelike asymmetric transmission of linearly polarized wave. It is composed of a pair of metallic two-turn spiral resonator on both sides of a dielectric substrate. The bottom pattern is formed by rotating an enantiometric form of the upper spiral resonator by 90°. This construction law distinguishes any previous design with only a mutual 90° twist or with only an enantiometric form [26]. As a consequence, the chirality will be further enhanced. The linearly polarized plane EM wave with polarization along x- or y-direction is normally impinged on the sample along z-direction. Since the line symmetry along both

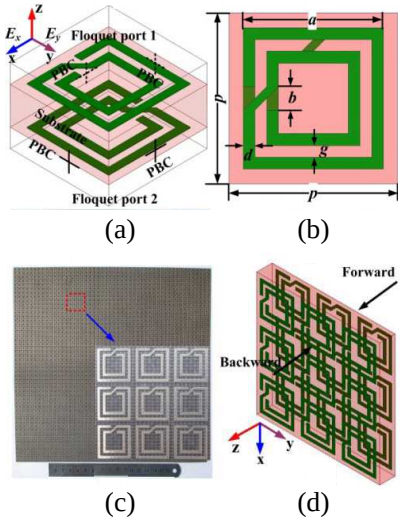

Figure 1. (a) Schematic and (b) parameters illustration of the chiral metamaterial unit cell. (c) Photograph of the fabricated sample slab, and (d) its orientation with the incident wave.

x and y directions of the spiral resonator is deliberately broken by the interconnection line between the big and small concentric rings with the same orientation, no line of mirror symmetry and any four-fold rotational symmetry (C4) can be observed. A pronounced structural two dimensional (2D) chirality is unambiguously carried out through the near-field interaction between the EM radiation and the interlayer building blocks. Due to the strong space-filling property of the spiral structure, the inductive current path is significantly extended and thus the resulting equivalent inductance and capacitance will be prominently increased in a limited volume [34]. Therefore, lower resonance of the CMM can be envisioned which equals the miniaturization of the meta-atom. Giant circular dichroism and optical activity will be engineered, respectively by tailoring EM response and mutual coupling in the upcoming two sections.

To characterize the chiral characteristic, we conducted all numerical simulations below in the commercial full-wave finite-element-method (FEM) EM field solver Ansoft HFSS. In the simulation setup in HFSS shown in Figure 1(a), the periodical boundary conditions (PBC) are adopted in the transverse xy plane while two floquet ports are assigned on the top and bottom boundary along z direction. By periodically arranging the well-designed atom-atom with a square period constant of p, a chiral slab with appealing circular behavior at

desired frequencies can be engineered. Figures 1(c) and (d) portray the photograph of the finally fabricated sample and its orientation with the incident wave.

3. COMPACT DUAL-BAND CIRCULAR POLARIZER

Based on the criterion described in previous section, we have constructed a CMM with giant circular dichroism over dual resonant bands. Its excellent performances deserve it to be a preferable candidate for dual-band circular polarizer application. In this particular design, the dielectric substrate is chosen as the commonly available inexpensive F4B substrate with a permittivity of $\varepsilon_r = 2.65$, a thickness of $h = 0.5\,\text{mm}$, and a loss tangent of 0.001, while the metallic layers on both sides are copper sheet with a thickness of $36\,\mu\text{m}$. Since the element spacing plays a dominant role in determination of the element coupling, it is carefully designed and optimized to consider a tradeoff among polarization extinction ratio, transmission coefficients and miniaturization. The final geometrical parameters of the chiral structure are designed as $p = 5.52\,\text{mm}$, $a = 4.4\,\text{mm}$, $b = 0.74\,\text{mm}$ and $d = g = 0.37\,\text{mm}$. For experimental use, we fabricate a well designed chiral sample that is composed of 50×50 unit cells and occupying an overall area of $276 \times 276\,\text{mm}^2$ through conventional printed circuit board technology, see Figure 1(c). It was measured through free-space EM transmission measurement in a microwave anechoic chamber, see Figure 2, where the sample was placed in the middle between a pair of double-ridged broadband horn antennas. Both antennas own VSWR < 2 over a wide frequency range of 1 to 18 GHz and face each other with a distance of 1.4 m to eliminate the near-field effects (direct coupling between two antennas). The time-domain gating strategy was used to eliminate the undesirable repetitively reflected EM waves. By changing the orientation of the two horn antennas to emit and

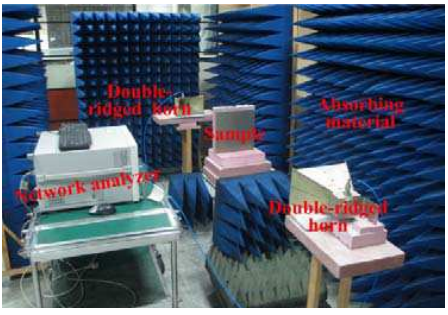

Figure 2. Experimental setup for the linear co- and cross-polarization transmission coefficients.

receive EM waves with different linear polarizations, four different linear transmission coefficients are recorded by the Agilent N5230C vector network analyzer. Then the linear-to-circular and circular-to-circular transmission coefficients can be easily transformed from the equations described in Section 2.

Since the structure lacks C4 symmetry, the electric response for the normally incident x-polarized wave distinguishes from that for the y-polarized wave. In this particular design, the giant circular dichroism and good performances of the circular polarizer are only valid for the y-polarized incident field. Figure 3 shows the simulated and measured four linear transmission coefficients as a function of frequency for the backward propagation ($-z$) with y-polarization. A reasonable agreement of results between simulation and measurement can be observed across the whole frequency range. Two resonant peaks (dips) are obviously observed around $f_1 = 8.08$ (8.05) and $f_2 = 9.9$ (9.83) GHz from the co- and cross-polarization transmission coefficients t_{yy} and t_{xy}. Slight frequency shift downward of about 60 MHz in the upper resonant band in the measurement case is due to the tolerances and random errors occurring in the fabrication and measurements. Numerical and experimental results both indicate that the peak of t_{xy} reaches at least -4.62 dB for both resonant bands. Therefore, high transformation efficiency is unambiguously demonstrated. The magnitude and phase difference of the co and cross-polarization transmission coefficients are depicted in Figure 4. As can be seen, the transmitted waves for the linear polarizations almost have identical amplitudes ($t_{xy}/t_{yy} = 1.12$ and 1.18) and a $-90°$ and $+90°$ phase difference at about 8.09 and 9.93 GHz, respectively,

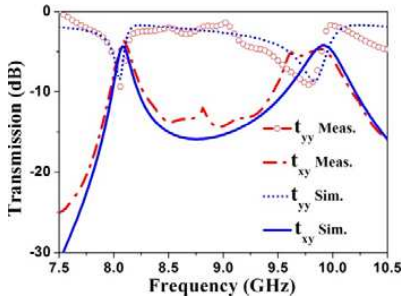

Figure 3. Simulated and measured four linear transmission coefficients for the backward propagation in y polarization.

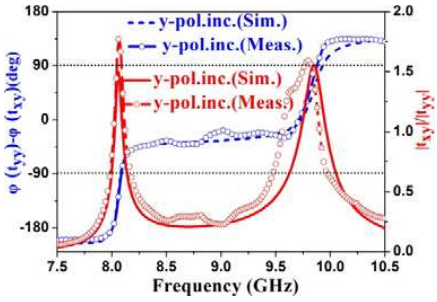

Figure 4. Comparison of simulated and measured phase and magnitude difference of t_{yy} and t_{xy}.

which suggests a nearly pure circular polarization wave is emitted. For the backward x-polarized incident wave (results not shown), two resonant peaks are also observed almost at the same frequencies with a slight frequency shift upwards measured by the $-90°$ and $+90°$ phase difference, however, only a 30% cross-polarizations transmission is achieved which is much lower than co-polarization, enabling an elliptically transmitted wave.

Figure 5 displays the simulated and measured LCP and RCP emitted wave transmission coefficients calculated from the two linear wave transmission coefficients. As is expected, two transmission dips at f_1 and f_2 indicate two distinct resonances. Numerical (experimental) results indicate that the transmitted RCP wave reaches a minimum value of -21.9 dB (-16.9 dB) at 8.09 GHz (8.1 GHz) while the LCP wave reaches a minimum value of -24.9 dB (-23.9 dB) at 9.94 GHz (9.9 GHz). At both frequencies, the transmission coefficients of the LCP and RCP wave are observed as -1.88 dB (-1.87 dB) and -1.8 dB (-1.85 dB), respectively, enabling large polarization extinction ratios of -20 (-15 dB) and 23 dB (21.8 dB) and pronounced circular dichroism at the above two frequencies. Therefore, at f_1, the LCP wave dominates the transmitted wave while at f_2 a prominent RCP wave is suggested at f_2. Consequently, the high conversion efficiency of the chiral structure is further validated by the relatively large transmitted RCP and LCP wave.

To further characterize the chiral characteristic, Figure 6 plots the consistent numerical and experimental polarization azimuth rotation angle and ellipticity in the case of y-polarization incidence. Referring to Figure 6(a), it is learned that the calculated (measured) value of η is $-39.9°$ ($-34.9°$), and $41°$ ($40.4°$) at 8.09 GHz (8.1 GHz), and 9.95 GHz (9.89 GHz), respectively, further confirming the nearly pure

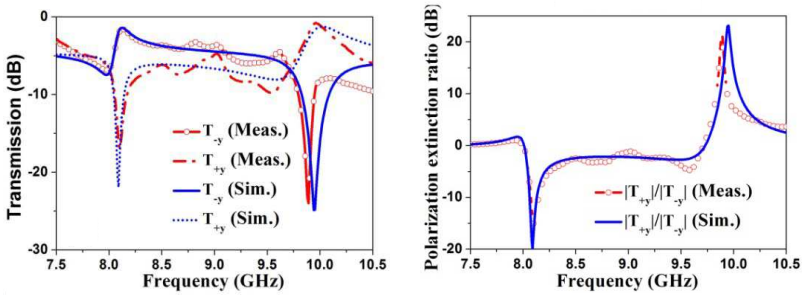

Figure 5. Comparison of simulated and measured linear-to-circular transmission coefficients. (a) Magnitude. (b) Difference.

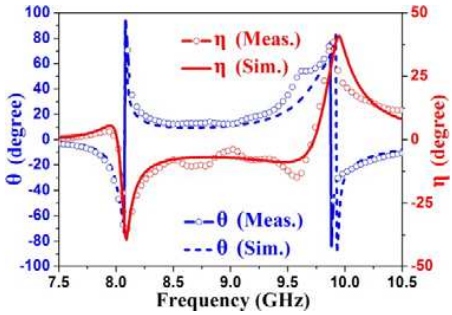

Figure 6. Simulated and measured polarization azimuth rotation angle and ellipticity of the CMM in the case of y-polarized incident wave.

LCP wave and RCP wave at f_1 and f_2, respectively. Note that $\eta = 45°$ corresponds to the pure circularly polarized wave whereas $\eta = 0°$ is the pure linearly polarized wave, and the wave is left handed elliptical when $\eta < 0°$, otherwise it is right handed elliptical. When $\eta = 0°$ at 8.01 GHz (7.99) and 9.73 (9.71) GHz, the simulated (measured) polarization azimuth rotation angles are found to be $\theta = -38.9°$ $(-35.3°)$ and $\theta = 45.3°$ $(54.8°)$, which suggests that the transmitted wave is still linear polarization with rotation angle θ. The rotated waves measured by θ are very comparable relative to any previously published article, revealing a promising optical activity.

Finally, the mechanism of the resonances and polarization transformation for the proposed dual-band CMM structure can be interpreted through longitudinal magnetic dipole to magnetic dipole coupling [1, 21, 24]. Figure 7 shows the phase of axial magnetic field and current distribution in two planes cutting through the top and bottom spiral layer. As is shown, the current flow at the two concentric rings of each layer is antiparallel at both frequencies, enabling two magnetic dipoles with the obviously antiparallel moments within both rings, see the phase of the magnetic field. For the low-frequency LCP resonance, the surface currents on both inner and outer ring of one spiral layer are in the same direction as those of the other twisted enantiometric pattern, which results in parallel magnetic dipole moments in outer and inner rings of both layers. On the other hand, the surface currents on the two layers are antiparallel for both rings for the upper-frequency RCP resonance, indicating antiparallel magnetic dipole moments in both layers. The distinguished current flow of the top-and-bottom layer at f_1 and f_2 gives rise to the different handness of the circularly transmitted waves at the two resonant frequencies. Moreover, the strong surface current density on the bottom layer with respect to that on the top layer interprets

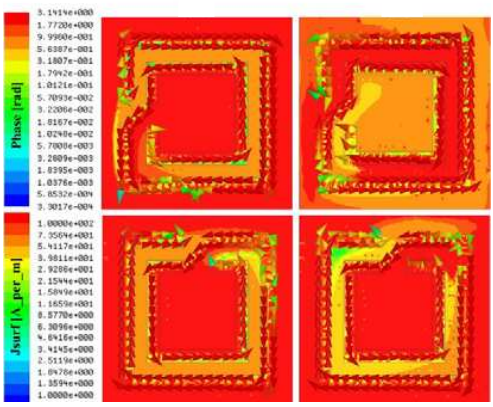

Figure 7. Axial magnetic field (phase) and surface current distribution of the proposed CMM in the case of y-polarized incident wave. (a) LCP wave at $f_1 = 8.08\,\text{GHz}$. (b) RCP wave at $f_2 = 9.94\,\text{GHz}$. Note that the arrows indicate the surface current directions. The top row is snapshot of the top pattern while the bottom row is that of the bottom pattern.

the strong interlayer coupling and thus the strong transmission conversion efficiency observed previously. Comparing to previous SRR structure [12–14, 30, 33], the interconnected spiral structure features extra noticeable compactness ($\lambda_0/6.73 \times \lambda_0/6.73 \times \lambda_0/74.3$), e.g., even achieves about 8% frequency reduction of the upper band relative to the smallest double SRR structure [24] with the same footprint on the same substrate, where λ_0 is the wavelength in free space evaluated at 8.08 GHz. Another major advantage is the additional resonant band introduced at higher frequencies.

4. NEAR DIODELIKE ASYMMETRIC TRANSMISSION FOR SPECTRUM FILTER

Asymmetric transmission for linear polarization is unusual and appealing polarization functionalities studied in recent years [11–15]. In [11], a thin structure composed of three-dimensional meta-atoms allowing asymmetric transmission for an arbitrary including linear polarization of the incident electromagnetic wave was proposed without any rotational symmetry. Afterwards, theoretical prediction and experimental realization on asymmetric transmission for linear polarization only were continuously reported by using gammadion structure [11] and SRR structure [12, 13], respectively. In [14],

the directionally asymmetric transmission of linearly and circularly polarized waves was suggested to be manipulated via angles of incidence. However, the cross-polarized conversion in above literature was insufficient. This is particularly true for the weak cross-polarization transmission(less than 0.3) of the asymmetric SRR whose element size reaches $\lambda_0/3.3$ at the resonance [14]. To realize a Diodelike asymmetric transmission, namely unity transmission of certain linear polarization in one direction while zero transmission in the opposite direction, electromagnetic wave tuning was suggested to be accompanied with the magnetoelectric coupling [15]. This strategy affords us indeed a versatile avenue to manipulate propagation of EM waves and would be excellent if the chiral element size was compact.

In this section, to examine the asymmetric effects we conduct a design aiming at the maximization of cross-polarized transmission for y-polarized backward incidence and also at the miniaturization of the meta-atoms. Like [11–15], asymmetric transmission is still a completely reciprocal phenomenon by efficiently tailoring the EM response and mutual coupling between the two spiral resonators on different layer investigated in Section 3. We modified previous design by changing the geometrical parameters of the chiral element and substrate board. Both copper chiral meta-atoms with a thickness of 36 µm and geometrical parameters of $p = 4.78\,\text{mm}$, $a = 4.4\,\text{mm}$, $b = 0.74\,\text{mm}$, and $d = g = 0.37\,\text{mm}$ are periodically patterned on both sides of the F4B substrate with a permittivity of $\varepsilon_r = 2.65$, a thickness of $h = 2\,\text{mm}$, and a loss tangent of 0.001. In the fabrication of the sample, a total of 50×50 unit cells are etched on an overall size of $239 \times 239\,\text{mm}^2$ substrate board.

Figure 8 depicts the simulated and measured transmission spectra of the four linear transmission coefficients for backward and forward propagations. Numerical and experimental results are in excellent consistency with each other across the whole frequency range. For the linear wave normally incident along the backward direction, the co-polarization components t_{yy} and t_{xx} are numerically observed the same while experimentally almost the same, whereas the cross-polarization waves t_{yx} and t_{xy} distinguish considerably from first to last. The y-polarized linear wave couples to the CMM though the spiral resonator and then converts mostly to x-polarization wave through the cross-coupling while in contrast the coupling of x-polarized linear wave to its cross-polarization is nearly blocked. Numerical (experimental) results indicate that t_{yy} and t_{xx} experience a minimum value of 0.12 (0.115) at 8.82 (8.81) GHz, while t_{xy} undergoes a resonant peak and reaches a maximum value of 0.91 (0.90) at 8.65 (8.66) GHz and t_{yx} is observed on the order of 0.02 (0.03) around these frequencies. The

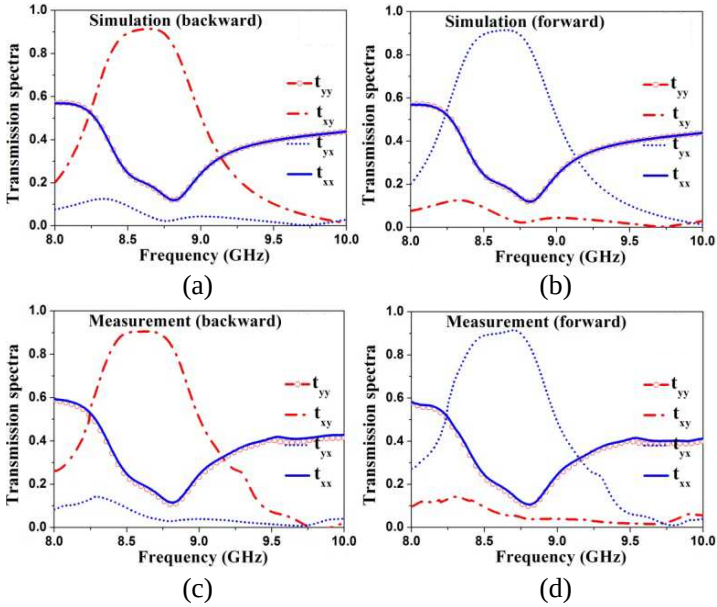

Figure 8. (a), (b) Simulated and (c), (d) measured transmission spectra of the four linear transmission coefficients for (a), (c) backward and (b), (d) forward propagations.

noticeable difference between t_{yx} and t_{xy} results in giant asymmetric transmission effect for the linear polarization, which is associated with the polarization conversion of the chiral medium [12]. On the contrary when the linear wave is normally incident along the forward propagation, almost the same results are expected except for the exchanged x and y-polarization components between the two cases. As a consequence, the transmission for linear polarization is proved asymmetric for both propagation and direction.

Figure 9 portrays the simulated and measured Δ parameters of the chiral medium in both linear and circular polarization bases. As is expected, the calculated (measured) magnitude of the Δ parameter in the linear polarization base reaches a positive maximum value of 0.83 (0.82) while a negative minimum value of near -0.83 (-0.82) at 8.66 (8.65) GHz for the y and x polarization, respectively, whereas that in the circular polarization base is observed near zero across the entire frequency range. Therefore, the asymmetric transmission is confirmed only for the linear polarization. The Δ parameter for the linear polarization is very comparable with respect to previous 0.64 in [12] and 0.55 in [13]. The huge asymmetric effects will also lead to the asymmetric total transmission of certain linearly polarized wave in two opposite directions. For verification, the total transmissions for y-

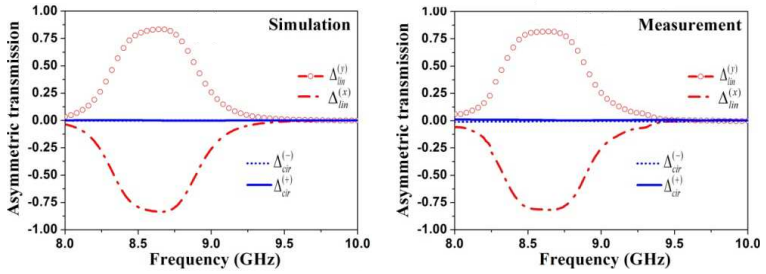

Figure 9. (a) Simulated and (b) measured Δ parameters of the chiral medium in both linear and circular polarization bases.

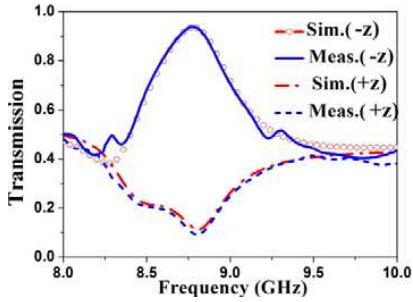

Figure 10. Simulated and measured total transmission for y-polarized incident wave along the backward and forward propagations.

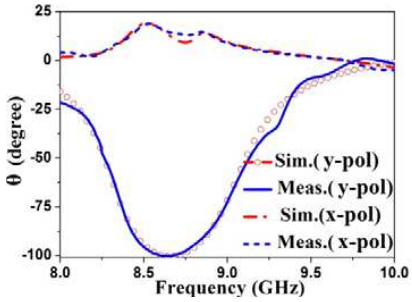

Figure 11. Simulated and measured polarization azimuth angle for x and y-polarized wave incident along the backward direction.

polarized incident wave along the backward and forward propagations are shown in Figure 10, where a reasonable agreement of results is obtained between simulation and measurement. Experimental results indicate that the backward total transmission reaches a peak value of 0.94 at 8.78 GHz while the forward total transmission approaches a minimum value of 0.1 at 8.8 GHz. The substantially different total transmission along the two opposite directions indicates a strong asymmetric factor of transmission.

Figure 11 compares the simulated and measured polarization azimuth angle of the emitted wave for both x and y-polarized wave incident along the backward direction. It is learned that the major polarization axis of the emitted wave for y polarization incidence undergoes clockwise rotation rapidly toward x axis ($-90°$), then reaches a negative maximum value of $-100.3°$ at 8.65 GHz and finally rotates counterclockwise rapidly back to y axis. However, a

considerably flat response of the polarization azimuth angle is observed for the emitted wave in the case of x polarization incidence. Therefore, the interlayer near-field coupling between two twisted layers also leads to the asymmetric optical activity for different polarizations. The resonant polarization conversion tailored by the EM coupling accounts for the high asymmetric factor.

Finally, we have conducted the evolution of electric fields in the incoming regime, outgoing regime and the substrate in Figure 12 to afford a direct and intuitionistic witness and understanding of the asymmetric transmission. The y-polarized wave incident along the backward and forward directions is considered for complementary analysis. For the backward incidence, the interaction of the y-polarized wave with the top spiral structure excites the magnetic resonance of the chiral structure and thus yields magnetic dipole moments. Then the corresponding dipole moment couples to the bottom layer and contributes to the conversion of two orthogonal linear polarizations. The field strength of the outgoing wave is on the order of 90% of incoming wave, coinciding well with the observed cross-coupled transmitted coefficients. The coupling process in forward incidence is the same as that in backward incidence but with different polarization conversion rate due to the bi-anisotropic responses to EM waves. As is shown, the resonant excitation and coupling of the magnetic dipole moment is prominently weak. The forwardly transmitted cross-polarization field intensity is only about 9.8% of the intensity of the incident wave, which again agrees well with the simulated and measured transmission coefficients. The size of the

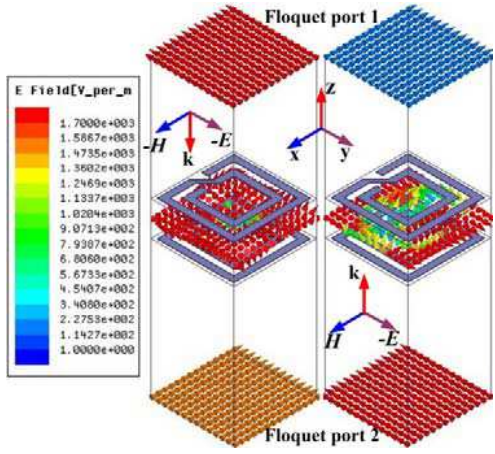

Figure 12. Snapshots of the electric-field distribution for y-polarized wave incident along the (a) backward and (b) forward directions at 8.65 GHz.

spiral element is assessed as $\lambda_0/7.3 \times \lambda_0/7.3 \times \lambda_0/17.3$ at 8.65 GHz. The near unity cross-polarization transmission coefficients of certain linear polarization wave in one direction of propagation while near zero transmission in the opposite direction reveal that the CMM is a good candidate for polarization spectrum filters and transparent polarization transformers.

5. CONCLUSIONS

In summary, we have proposed and comprehensively characterized an alternative compact CMM with additional line asymmetry. We demonstrate numerically and experimentally that giant circular dichroism and near diodelike asymmetric transmission can be implemented through optimally tailoring EM response and mutual coupling of bilayered spiral resonators with specific configuration. Giant optical activity is also realized accompanied with above two fundamental behaviors of the CMM. The abnormal EM behavior enables them to be preferably selected for a circular polarizer and an asymmetric spectrum filter. Moreover, the interconnected spiral ring features dual-band resonance and very compact package, and thus affords a great degree of flexibility in multifunction design and goes beyond previous chiral structures. The operation frequency of the proposed CMM can also be scaled to other EM spectrum due to the geometry scalability. Our study enriches the asymmetric transmission effect and chiral characteristics through a metamaterial design.

ACKNOWLEDGMENT

This work was supported in part by the National Natural Science Foundation of China under Grant No. 61372034, in part by the foundation for Excellent Doctoral Dissertation of Air Force Engineering University under Grant No. KGD080913001, and in part by the Innovation Foundation for Postgraduate's Dissertation of Air Force Engineering University under Grant No. DY12101. The authors also acknowledge Professor Tie Jun Cui for experimental apparatus afforded in the measurements.

REFERENCES

1. Decker, M., R. Zhao, C. M. Soukoulis, S. Linden, and M. Wegener, "Twisted split-ring-resonator photonic metamaterial with huge optical activity," *Opt. Lett.*, Vol. 35, 1593–1595, 2010.

2. Kwon, D. H., P. L. Werner, and D. H. Werner, "Optical planar chiral metamaterial designs for strong circular dichroism and polarization rotation," *Opt. Express*, Vol. 16, 11802–11807, 2008.
3. Rogacheva, A. V., V. A. Fedotov, A. S. Schwanecke, and N. I. Zheludev, "Giant gyrotropy due to electromagnetic-field coupling in a bilayered chiral structure," *Phys. Rev. Lett.*, Vol. 97, 177401, 2006.
4. Pendry, J. B., "A chiral route to negative refraction," *Science*, Vol. 306, No. 5700, 1353–1355, 2004.
5. Plum, E., J. Zhou, J. Dong, V. A. Fedotov, T. Koschny, C. M. Soukoulis, and N. I. Zheludev, "Metamaterial with negative index due to chirality," *Phys. Rev. B*, Vol. 79, 035407, 2009.
6. Wongkasem, N., A. Akyurtlu, K. A. Marx, Q. Dong, J. Li, and W. D. Goodhue, "Development of chiral negative refractive index metamaterials for the terahertz frequency regime," *IEEE Trans. Antennas Propag.*, Vol. 55, No. 11, 3052–3062, Nov. 2007.
7. Wu, Z., B. Q. Zhang, and S. Zhong, "A double-layer chiral metamaterial with negative index," *Journal of Electromagnetic Waves and Applications*, Vol. 24, No. 7, 983–992, 2010.
8. Li, J., F.-Q. Yang, and J.-F. Dong, "Design and simulation of L-shaped chiral negative refractive index structure," *Progress In Electromagnetics Research*, Vol. 116, 395–408, 2011.
9. Zarifi, D., M. Soleimani, V. Nayyeri, and J. Rashed-Mohassel, "On the miniaturization of semiplanar chiral metamaterial structures," *IEEE Trans. Antennas Propag.*, Vol. 60, No. 12, 5768–5776, 2012.
10. Plum, E., V. A. Fedotov, and N. I. Zheludev, "Planar metamaterial with transmission and reflection that depend on the direction of incidence," *Appl. Phys. Lett.*, Vol. 94, 131901, 2009.
11. Menzel, C., C. Helgert, C. Rockstuhl, E.-B. Kley, A. Tünnermann, T. Pertsch, and F. Lederer, "Asymmetric transmission of linearly polarized light at optical metamaterials," *Phys. Rev. Lett.*, Vol. 104, 253902, 2010.
12. Huang, C., Y. Feng, J. Zhao, Z. Wang, and T. Jiang, "Asymmetric electromagnetic wave transmission of linear polarization via polarization conversion through chiral metamaterial structures," *Phys. Rev. B*, Vol. 85, 195131, 2012.
13. Cheng, Y., Y. Nie, X. Wang, and R. Gong, "An ultrathin transparent metamaterial polarization transformer based on a twist-split-ring resonator," *Appl. Phys. A*, Vol. 111, 209–215, 2013.
14. Shi, J. H., Z. Zhu, H. F. Ma, W. X. Jiang, and T. J. Cui, "Tunable symmetric and asymmetric resonances in an asymmetrical split

ring metamaterial," *J. Appl. Phys.*, Vol. 112, 073522, 2012.

15. Mutlu, M., A. E. Akosman, A. E. Serebryannikov, and E. Ozbay, "Diodelike asymmetric transmission of linearly polarized waves using magnetoelectric coupling and electromagnetic wave tunneling," *Phys. Rev. Lett.*, Vol. 108, 213905, 2012.
16. Gansel, J. K., M. Thiel, M. S. Rill, M. Decker, K. Bade, V. Saile, G. von Freymann, S. Linden, and M. Wegener, "Gold helix photonic metamaterial as broadband circular polarizer," *Science*, Vol. 325, No. 5947, 1513–1515, 2009.
17. Euler, M., V. Fusco, R. Cahill, and R. Dickie, "325 GHz single layer sub-millimeter wave FSS based split slot ring linear to circular polarization convertor," *IEEE Trans. Antennas Propag.*, Vol. 58, No. 7, 2457–2459, 2010.
18. Wu, C., H. Li, X. Yu, F. Li, H. Chen, and C. T. Chan, "Metallic helix array as a broadband wave plate," *Phys. Rev. Lett.*, Vol. 107, 177401, 2011.
19. Zhao, Y., M. A. Belkin, and A. Alù, "Twisted optical metamaterials for planarized ultrathin broadband circular polarizers," *Nat. Commun.*, Vol. 3, 870, 2012, Doi: 10.1038/ncomms1877,
20. Ye, Y., X. Li, F. Zhuang, and S.-W. Chang, "Homogeneous circular polarizers using a bilayered chiral metamaterial," *Appl. Phys. Lett.*, Vol. 99, 031111, 2011.
21. Mutlu, M., A. E. Akosman, A. E. Serebryannikov, and E. Ozbay, "Asymmetric chiral metamaterial circular polarizer based on four U-shaped split ring resonators," *Opt. Lett.*, Vol. 36, 1653–1655, 2011.
22. Ma, X., C. Huang, M. Pu, C. Hu, Q. Feng, and X. Luo, "Multi-band circular polarizer using planar spiral metamaterial structure," *Opt. Express*, Vol. 20, No. 14, 16050–16058, 2012.
23. Xu, H.-X., G.-M. Wang, M. Q. Qi, T. Cai, and T. J. Cui, "Compact dual-band circular polarizer using twisted Hilbert-shaped chiral metamaterial," *Opt. Express*, Vol. 21, No. 21, 24912–24921, 2013.
24. Yana, S. and G. A. E. Vandenbosch, "Compact circular polarizer based on chiral twisted double split-ring resonator," *Appl. Phys. Lett.*, Vol. 102, 103503, 2013.
25. Chin, J. Y., J. N. Gollub, J. J. Mock, R. Liu, C. Harrison, D. R. Smith, and T. J. Cui, "An efficient broadband metamaterial wave retarder," *Opt. Express*, Vol. 17, 7640–7647, 2009.
26. Ye, Y. and S. He, "90° polarization rotator using a bilayered chiral metamaterial with giant optical activity," *Appl. Phys. Lett.*,

Vol. 96, 203501, 2010.

27. Song, K., X. P. Zhaoa, Q. H. Fu, Y. H. Liu, and W. R. Zhu, "Wide-angle 90°-polarization rotator using chiral metamaterial with negative refractive index," *Journal of Electromagnetic Waves and Applications*, Vol. 26, Nos. 14–15, 1967–1976, 2012.
28. Song, K., Y. H. Liu, Q. Fu, X. P. Zhao, C. R. Luo, and W. R. Zhu, "90° polarization rotator with rotation angle independent of substrate permittivity and incident angles using a composite chiral metamaterial," *Opt. Express*, Vol. 21, 7439–7446, 2013.
29. Mutlu, M. and E. Ozbay, "A transparent 90° polarization rotator by combining chirality and electromagnetic wave tunneling," *Appl. Phys. Lett.*, Vol. 100, 051909, 2012.
30. Shi, J. H., H. F. Ma, W. X. Jiang, and T. J. Cui, "Multiband stereometamaterial-based polarization spectral filter," *Phys. Rev. B*, Vol. 86, 035103, 2012.
31. Zari, D., H. Oraizi, and M. Soleimani, "Improved performance of circularly polarized antenna using semi-planar chiral metamaterial covers," *Progress In Electromagnetics Research*, Vol. 123, 337–354, 2012.
32. Monzon, C. and D. W. Forester, "Negative refraction and focusing of circularly polarized waves in optically active media," *Phys. Rev. Lett.*, Vol. 95, 123904, 2005.
33. Wang, B., T. Koschny, and C. M. Soukoulis, "Wide-angle and polarization-independent chiral metamaterial absorber," *Phys. Rev. B*, Vol. 80, 033108, 2009.
34. Xu, H.-X., G.-M. Wang, M.-Q. Qi, J.-G. Liang, J.-Q. Gong, and Z.-M. Xu, "Triple-band polarization-insensitive wide-angle ultra-miniature metamaterial transmission line absorber," *Phys. Rev. B*, Vol. 86, 205104, 2012.
35. Xu, H.-X., G.-M. Wang, M. Q. Qi, L. Li, and T. J. Cui, "Three-dimensional super lens composed of fractal left-handed materials," *Adv. Opt. Mater.*, Vol. 1, 495–502, 2013.
36. Xu, H. X., G. M. Wang, and M. Q. Qi, "Hilbert-shaped magnetic waveguided metamaterials for electromagnetic coupling reduction of microstrip antenna array," *IEEE Trans. Magnetics*, Vol. 49, No. 4, 1526–1529, 2013.
37. Baena, J. D., J. Bonache, F. Martín, R. M. Sillero, F. Falcone, T. Lopetegi, et al., "Equivalent-circuit models for split-ring resonators and complementary split-ring resonators coupled to planar transmission lines," *IEEE Trans. Microw. Theory Tech.*, Vol. 53, No. 4, 1451–1461, 2005.